ICES Journal of Marine Science

ICES Journal of Marine Science (2015), 72(6), 1961–1970. doi:10.1093/icesjms/fsv006

Contribution to the Themed Section: '*Revisiting Sverdrup's Critical Depth Hypothesis*'

Original Article

Characterizing upper-ocean mixing and its effect on the spring phytoplankton bloom with *in situ* data

Sarah R. Brody* and M. Susan Lozier

Department of Earth and Ocean Sciences, Duke University, Durham, NC 27708, USA

**Corresponding author: tel/fax: +1 919 613 2115; e-mail: sarah.brody@duke.edu*

Brody, S. R., and Lozier, M. S. Characterizing upper-ocean mixing and its effect on the spring phytoplankton bloom with *in situ* data. – ICES Journal of Marine Science, 72: 1961 – 1970.

Received 29 May 2014; revised 2 January 2015; accepted 5 January 2015; advance access publication 4 February 2015.

Since publication, the Sverdrup hypothesis, that phytoplankton are uniformly distributed within the ocean mixed layer and bloom once the ocean warms and stratifies in spring, has been the conventional explanation of subpolar phytoplankton spring bloom initiation. Recent studies have sought to differentiate between the actively mixing section of the upper ocean and the uniform-density mixed layer, arguing, as Sverdrup implied, that decreases in active mixing drive the spring bloom. In this study, we use *in situ* data to investigate the characteristics and depth of active mixing in both buoyancy- and wind-driven regimes and explore the idea that the shift from buoyancy-driven to wind-driven mixing in the late winter or early spring creates the conditions necessary for blooms to begin. We identify the bloom initiation based on net rates of biomass accumulation and relate changes in the depth of active mixing to changes in biomass depth profiles. These analyses support the idea that decreases in the depth of active mixing, a result of the transition from buoyancy-driven to wind-driven mixing, control the timing of the spring bloom.

Keywords: Lagrangian floats, North Atlantic Bloom experiment, Ocean turbulence, phytoplankton, spring bloom, Sverdrup hypothesis.

Introduction

The timing of the subpolar spring phytoplankton bloom has long been of interest to oceanographers due to its impact on carbon export (Stramska *et al.*, 1995; Sabine *et al.*, 2004; Lutz *et al.*, 2007) and upper trophic level species recruitment (Platt *et al.*, 2003; Edwards and Richardson, 2004; Koeller *et al.*, 2009). In his seminal 1953 paper, Harald Sverdrup hypothesized that because phytoplankton are uniformly distributed within the ocean mixed layer, the spring shoaling of this mixed layer increases available light to a level at which the phytoplankton population can grow (Sverdrup, 1953). While Sverdrup defined the term "mixed layer" as the section of the water column exhibiting both active turbulence and homogenous density, contemporary studies in support of the Sverdrup Hypothesis have generally used density-based criteria only to define the mixed layer (e.g. Follows and Dutkiewicz, 2001; Siegel *et al.*, 2002; Henson *et al.*, 2009), and have linked the timing of the spring bloom to ocean surface warming (Follows and Dutkiewicz, 2001; Henson *et al.*, 2006). More recent work has focused on the possibility that decreases in active turbulence within the mixed layer, rather than decreases in the mixed layer itself, create the conditions necessary for bloom onset (Huisman *et al.*, 1999; Chiswell, 2011; Taylor and Ferrari, 2011; Chiswell *et al.*, 2013). This decrease has been attributed to the shutdown of turbulent convection after heat fluxes become positive (Taylor and Ferrari, 2011) and also to decreases in the local wind strength (Chiswell, 2011; Chiswell *et al.*, 2013). Because phytoplankton blooms that occur when the ocean mixed layer is deep encounter reduced barriers to sinking and thus export higher amounts of carbon than blooms that occur in shallow mixed layers (Stramska *et al.*, 1995), this distinction has important consequences for the marine carbon cycle.

Other recent work has focused on localized increases in water column stratification by means other than warming as a driver of blooms. Specifically, it has been suggested that lateral density gradients are converted to vertical density gradients by submesoscale eddies within the mixed layer, and that this increase in stratification can initiate blooms (Mahadevan *et al.*, 2012). Finally, while contemporary bloom phenology studies typically use surface chlorophyll from satellite data to examine the phytoplankton seasonal cycle (Platt *et al.*, 2009; Cole *et al.*, 2012; Racault *et al.*, 2012; Sapiano

et al., 2012; Brody *et al.*, 2013), a series of studies (Behrenfeld, 2010; Boss and Behrenfeld, 2010; Behrenfeld *et al.*, 2013) has drawn attention to the fact that the original work by Sverdrup focused on the rate of net biomass accumulation within the water column. The use of this metric has led to an alternative hypothesis regarding the phytoplankton seasonal cycle (Behrenfeld, 2010; Boss and Behrenfeld, 2010; Behrenfeld *et al.*, 2013): positive net accumulation rates are driven by the deepening of the mixed layer in winter, dilution of the plankton population, and consequent decreases in zooplankton grazing pressure.

Brody and Lozier (2014) (hereafter BL14) investigated several proposed drivers of the subpolar spring bloom in the North Atlantic: shoaling seasonal mixed layers (Follows and Dutkiewicz, 2001; Siegel *et al.*, 2002; Henson *et al.*, 2009), the onset of positive heat fluxes (Taylor and Ferrari, 2011), and decreases in wind strength (Chiswell, 2011; Chiswell *et al.*, 2013). BL14 compared these mechanisms to a new framework for the North Atlantic bloom initiation: that blooms begin when the dominant mixing length scale (L_{mix}), or depth of active mixing, in the upper ocean decreases. BL14 found that decreases in L_{mix} are a better predictor of bloom initiation than decreases in the mixed layer depth, the onset of positive heat fluxes, or decreases in wind strength. They also found that decreases in L_{mix} generally occur after the shift from buoyancy-driven to wind-driven mixing in the upper ocean, likely because strongly negative surface buoyancy fluxes generate larger, more coherent vertical eddies compared with those generated by wind forcing, which then reduce the light exposure of phytoplankton within the upper ocean. Essentially, BL14 clarified and expanded upon the light-limitation-based explanation of bloom initiation described in the Sverdrup hypothesis by estimating a depth of turbulent mixing that differs at times from the density-defined mixed-layer depth, and providing a mechanism for bloom initiation that does not depend on the onset of positive heat fluxes (net ocean surface warming).

The BL14 framework was tested using satellite data to identify the spring bloom and surface reanalysis data to estimate mixing length scales, thus leaving open questions regarding how well the L_{mix} model estimates the depth of active mixing, and whether the shift from buoyancy-driven to wind-driven mixing causes the active mixing depth to shoal. *In situ* datasets provide a unique opportunity to more closely examine the BL14 framework by allowing for the estimation of mixing from measurements in the upper ocean rather than relying on information from surface forcing fields. Specifically, we use *in situ* data to (i) assess whether surface forcing data can be used to accurately estimate the depth of L_{mix} under different conditions; (ii) further characterize differences and similarities in buoyancy-driven and wind-driven mixing to determine whether and how buoyancy forcing drives deeper mixing than wind forcing; and (iii) investigate whether decreases in L_{mix} precede the initiation of the spring bloom, as measured using depth-resolved biomass records.

To answer the first two questions, we employ data from autonomous Lagrangian floats. Because these floats are designed to be neutrally buoyant (D'Asaro *et al.*, 1996), they can follow the three-dimensional motions of water parcels and have been used to examine turbulence within the upper ocean during a variety of mixing regimes. For this study, we use data from the Labrador Sea Experiment (Krahmann *et al.*, 2003), when deep convection drove turbulent mixing (Steffen and D'Asaro, 2002), and from the North Atlantic Bloom 2008 experiment (Fennel *et al.*, 2011), during which mixing was primarily wind-driven (Mahadevan *et al.*, 2012). By assuming that these Lagrangian floats simulate the trajectories of particles within the upper ocean (Harcourt *et al.*, 2002; D'Asaro, 2008), we use their vertical paths to observe the strength and depth of active mixing in the ocean in buoyancy-driven and wind-driven mixing environments. To answer the third question, we examine changes in depth-integrated biomass using biological data collected during a subpolar spring bloom as part of the North Atlantic Bloom 2008 experiment.

Data and methods

Data

Float data

We utilize data from two field programmes. The Labrador Sea Deep Convection Experiment (Krahmann *et al.*, 2003) deployed 25 Lagrangian floats during winters of 1997/1998 in the Labrador Sea (52–56°W, 56–59°N). Floats drifted for ~2 months, recording temperature and pressure at 5 min intervals, and position at 4 h intervals (see Steffen and D'Asaro, 2002 for further details on float mechanics and experiment design). We additionally use data from 36 PALACE floats (Davis *et al.*, 1992; Lavender *et al.*, 2000), also deployed during the Labrador Sea Experiment, which parked at varying depths in the Labrador Sea (400, 700, and 1500 m) and periodically surfaced to record temperature and salinity profiles.

In the North Atlantic Bloom 2008 Experiment (NAB08), one Lagrangian float was deployed during the months of April and May 2008 in the subpolar North Atlantic south of Iceland (58.5–62.5°N, 18–28°W) (Fennel *et al.*, 2011; Mahadevan *et al.*, 2012). This float alternated between drifting within the mixed layer, profiling, and autoballasting. During all modes, the float recorded temperature, salinity, and position data every 50–60 s. In both Lagrangian float experiments, the floats were designed to be neutrally buoyant through adjustable compressibility and high drag (D'Asaro *et al.*, 1996; D'Asaro, 2003).

Glider data

The NAB08 experiment deployed four Seagliders (Eriksen *et al.*, 2001) on paths following the Lagrangian float. The Seagliders continuously profiled the upper ocean, collecting approximately four profiles per day between 0 and 1000 m. The Seagliders measured temperature, salinity, and pressure, as well as chlorophyll *a* fluorescence, and backscatter at 700 nm wavelength calibrated to ship-based observations (see Briggs *et al.*, 2011 for further details on the Seaglider instrumentation). Consistent with previous work on the NAB08 data (e.g. Briggs *et al.*, 2011; Cetinic *et al.*, 2012), we use both the chlorophyll *a* fluorescence and backscatter at 700 nm (bbp(700)) as proxies for phytoplankton biomass (Behrenfeld *et al.*, 2005).

To facilitate comparison between derived physical variables (e.g. mixed layer depths) and derived biological variables (e.g. net biomass accumulation rates), we process the physical (temperature, salinity, density) and biological (chlorophyll fluorescence and bbp (700)) observations from the gliders using the same methods. Following Briggs *et al.* (2011), we process the data by first smoothing the profiles using sequential five-point running median filters and seven-point running mean filters. For ease of comparison with surface forcing data, which has a 1-d temporal resolution, and to highlight variability in biomass and density at the scale of the water column, we average the data into 1-d, 10-m bins, then smooth with 2-d, 50-m running means to further filter out submesoscale

variability (Briggs *et al.*, 2011). We then average daily data from all gliders.

Surface forcing data

We use three surface forcing products containing both winds and heat fluxes: Objectively Analyzed Air-Sea Fluxes (OAFlux) (Yu and Weller, 2007; oaflux.whoi.edu), NCEP-NCAR reanalysis 2 (Kanamitsu *et al.*, 2002; http://www.esrl.noaa.gov/psd), and ECMWF-ERA-Interim daily fields (data-portal.ecmwf.int). All heat flux and wind products are at daily resolution, with spatial resolution varying from 0.75 to 2.6°. We also use one wind-only product from the NOAA WaveWatch III hindcast data (http://polar.ncep.noaa.gov/waves), which is available at a higher spatial and temporal resolution (0.5°, 3-h resolution). Finally, we use photosynthetically available radiation (PAR) obtained from 9-km, 8-d SeaWiFS data, via the Giovanni data portal (http://disc.sci.gsfc.nasa.gov/giovanni/). We obtained all surface forcing data for the period of the NAB08 experiment. Because the daily averaged distance between the float and the averaged position of the four Seagliders (maximum distance of 1.1°; mean distance of 0.41°) is comparable with both the spatial resolution of the surface forcing data and the distance between any two gliders on a given day (maximum distance of 2.3°; mean distance of 0.49°), we linearly interpolate the gridded values of the surface forcing data to the position of the Lagrangian float.

Upper-ocean vertical velocities

Observed

For both Lagrangian float datasets (Labrador Sea and NAB08), we calculate vertical velocities, w, at each time step using centred differencing of the depth and time records. We calculate turbulent vertical velocities using $w' = w - \bar{w}$. Because we focus on changes in vertical velocities at the timescale of phytoplankton growth (days) $\bar{w}$ is computed as a daily mean. For the NAB08 data, we additionally calculate the daily rms-vertical velocity, w_{rms}, for n daily measurements using $w_{\mathrm{rms}} = \sqrt{\sum (w_n - \bar{w})^2/n}$. In the Labrador Sea Experiment, Lagrangian floats were placed below the mixed layer in fall, and were entrained into the mixed layer as surface cooling strengthened and mixing deepened (Steffen and D'Asaro, 2002); we therefore exclude data collected before the entrainment of the floats into the convective layer (approximately the first half of the 1998 float records, as seen in Steffen and D'Asaro, 2002, figures 6 and 7) and after heat fluxes became positive (after 8 March for 1997, after 2 March for 1998) to ensure that upper-ocean mixing was buoyancy-driven during the period of analysis. Given these two conditions, no data from the 1998 floats were used in our analysis. For the NAB08 experiment, to ensure that we are examining wind-driven mixing, we exclude the period of the record during which heat fluxes were negative (before Day 13) for the analysis in Figure 2c. However, we use the entire NAB08 float depth record in to calculate w_{rms} in Figure 3b.

Estimated

We estimate the wind-driven vertical velocity, $w^\star$, from 10-m wind speeds (U_{10}), using $w_*^2 = \rho_a/\rho_w C_D U_{10}^2$, derived from the definition of windstress, where ρ_a and ρ_w are the densities of the air and the surface water, respectively, and C_D is the drag coefficient, calculated as a function of wind speed (Hersbach, 2011). We estimate buoyancy-driven vertical velocity, w_b, during periods of negative heat flux, using the relationship, verified in laboratory (Deardorff and Willis, 1985; Fernando *et al.*, 1991), field (Steffen and D'Asaro, 2002), and modelling (Deardorff, 1972; Molemaker and Dijkstra, 1997) studies, between w_b and surface buoyancy forcing (B_o). Steffen and D'Asaro (2002) tested several models relating w_b and B_0 and found the best predictive skill with the model $w_b = a(HB_o)^{1/3} + w_o$, where H is the mixed-layer depth and a and w_o are empirical constants. Following Steffen and D'Asaro (2002), we calculated a and w_o using a linear fit of $(HB_o)^{1/3}$ onto w_{rms} to obtain values of $a = 0.46$ and $w_o = 0.009$.

Mixed layer depth, H, and buoyancy frequency (N^2)

For both the Labrador Sea and NAB08 experiments, we calculate H using a density difference from the surface criteria, or density threshold. Because many different density thresholds have been used in previous studies to calculate mixed layer depths (see Holte and Talley, 2009 for a review), we choose two thresholds, 0.03 and 0.125 kg m^{-3}, to ensure that our findings are not sensitive to the choice of mixed layer depth definition. Mixed layer depths calculated with the 0.03 and 0.125 kg m^{-3} density thresholds are comparable with mixed layer depths calculated using the Holte and Talley (2009) density algorithm and a density gradient method (Figure 1), so our results using these two thresholds are likely insensitive to the method for determining the mixed layer depth. We use the PALACE floats to calculate daily mixed layer depths during the Labrador Sea experiment, with the surface density taken from the 13-m PALACE measurement. We average all H measurements derived from PALACE profiles recorded within the temporal and spatial range of the Lagrangian floats to create a mixed layer depth time series for the segment of the Lagrangian float record used in this study. Because 23 February and 5 March did not contain reliable PALACE profiles, we estimate H on those dates by the average of the surrounding days. For the NAB08 experiment, we use the binned daily density profiles from

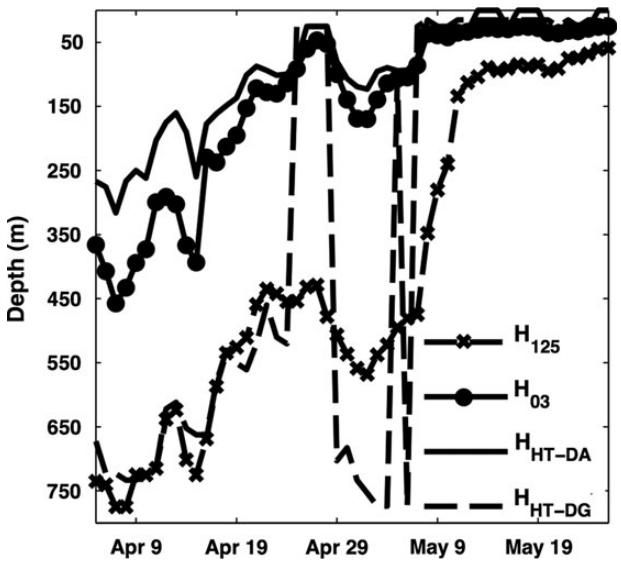

Figure 1. Mixed layer depths (H) calculated using the 0.03 and 0.125 kg m^{-3} density difference criteria (H_{03} and H_{125}) compared with mixed layer depths calculated using the Holte – Talley density algorithm (H_{DA}; Holte and Talley, 2009) and a maximum density gradient method, also from Holte and Talley (2009), H_{DG}, all calculated over the period of the North Atlantic Bloom 2008 experiment.

the glider records to calculate H, determining the surface density from the top bin (0–10 m).

We calculate the daily average N^2 for the NAB08 data over the maximum daily depth of the NAB08 Lagrangian float using the GSW MATLAB oceanographic toolbox (McDougall and Barker, 2011) and the binned glider temperature and salinity profiles.

Active mixing depth, L_{mix}

We calculate L_{mix} for the NAB08 period using the method outlined in BL14 for each of the three surface forcing products, and for each of the two mixed layer depth definitions, creating a total of six L_{mix} estimates. We define L_{mix} for three cases. In Case 1, where buoyancy-driven mixing dominates, L_{mix} is equal to the mixed layer depth (Taylor and Ferrari, 2011), H. In Case 2, where wind-driven mixing dominates in the presence of weak buoyancy forcing, L_{mix} is equal to the Ekman length scale (Denman and Gargett, 1983; Wang and Huang, 2003), L_{EK}. To calculate L_{EK}, we use $L_{EK} = \gamma(w_*)/f$, where f is the Coriolis parameter (1.27×10^{-4} s^{-1}) and γ is an empirical constant, for which we use a value of 0.5 (Wang and Huang, 2003). Finally, in Case 3, where wind-driven mixing dominates in the presence of strongly positive buoyancy forcing, L_{mix} is equal to the Ozmidov length scale (Denman and Gargett, 1983; Riley and Lelong, 2000), $L_{OZ} = (2\pi)\epsilon^{1/2}N^{-3/2}$, where ϵ is the rate of turbulent kinetic energy dissipation and is equal to $w_*^3/\kappa z$ at depth z, where $\kappa = 0.41$ is the Von Kármán constant. We base the transition between these cases on the relative strengths of wind and buoyancy forcing, as parameterized by the magnitude of the Obukhov length scale, $L_{OB} = -w_*^3/\kappa B_o$, where B_o is the surface buoyancy flux and is directly proportional to the surface heat flux (Phillips, 1977; Taylor and Ferrari, 2011).

Phytoplankton accumulation rates (r) and bloom period

We use both the daily chlorophyll fluorescence and bbp(700) profiles from the binned and processed NAB08 Seaglider data to calculate phytoplankton net accumulation rates, r, from the daily biomass rate of change (Behrenfeld, 2010; Boss and Behrenfeld, 2010; Behrenfeld *et al.*, 2013). Briefly, the definition of r we use accounts for phytoplankton growth occurring below the surface of the ocean and at times occurring deeper than the mixed layer depth by using three criteria for r. When mixed layers are deep and constant or deepening, r is calculated from biomass integrated to the depth of the mixed layer, consistent with the original Sverdrup hypothesis. When mixed layers are shallow, r is calculated from biomass integrated to the depth of a threshold isolume, above which phytoplankton have sufficient light to grow, to account for phytoplankton growth below a shallow mixed layer. Finally, when mixed layers are deep but shoaling, r is calculated from biomass averaged within the mixed layer, to exclude the portion of the phytoplankton population being detrained from the mixed layer and thus no longer actively growing. Further details can be found in Boss and Behrenfeld (2010).

We use H_{03} to calculate r: r calculated with H_{125} shows qualitatively similar patterns, but with slightly more variability in terms of whether r is positive or negative on any given day. We calculate the depth of the threshold isolume (z_{415}) as $z_{415} = \log(0.415/0.98PAR)(z_{eu}/\log(0.01))$ (Boss and Behrenfeld, 2010), where 0.415 mol quanta m^{-2} d^{-1} is the lowest PAR value that can support phytoplankton growth (Letelier *et al.*, 2004), and z_{eu} is the depth of the euphotic layer, calculated using surface chlorophyll concentrations (Morel *et al.*, 2007).

We then use the r record to identify the period of the spring bloom captured in the NAB08 record. Several methods exist to define the initiation of the subpolar spring phytoplankton bloom, and the selection of the method can depend on the question being asked (Brody *et al.*, 2013). To capture the start of a seasonal, rather than transient, bloom, we define the bloom as the period of sustained positive rates of biomass accumulation (Brody and Lozier, 2014), meaning that r calculated either with chlorophyll fluorescence or bbp(700) cannot be negative for >1 consecutive day during the bloom period. Therefore, we set the bloom initiation date to occur immediately after the last instance in which r is negative for two consecutive days, and the bloom termination date to occur immediately before r again becomes negative for two consecutive days.

Uncertainty in the calculation of r comes the fact that the 0.415 threshold PAR value was derived from measurements in the tropical Pacific Ocean, and thus likely represents a shallow estimate of the threshold isolume for subpolar phytoplankton (Boss and Behrenfeld, 2010). However, because the threshold isolume is only used in the r calculation once the mixed layer depth has become very shallow, this uncertainty only affects the end of the r record. We compared the threshold isolume with the euphotic depth (z_{eu}) and found very small differences between the two depths (see Figure 4). Additionally, r calculated with z_{eu} only differs from r calculated with z_{415} after Day 33 of the NAB08 record, within 1 day of the bloom termination, and only differs in magnitude, rather than sign. The choice of z_{415} to calculate r therefore has no effect on the date of the bloom initiation and termination.

Results

Assessment of estimated L_{mix}

We first use Lagrangian float paths to assess the BL14 estimate of the active mixing layer (L_{mix}) during buoyancy-driven mixing, where L_{mix} is equal to the mixed layer depth, H, and wind-driven mixing, where L_{mix} is equal to the Ekman depth, L_{EK}. In both cases, we use the daily maximum depth recorded by the Lagrangian floats (D_{max}) to estimate the depth of the active mixing layer from the float data. Although these datasets were collected at different times and at different locations in the subpolar North Atlantic, they each provide an example of what mixing might look like under buoyancy-driven and wind-driven conditions.

In the wind-driven case (the NAB08 record after 17 April, Figure 2a), we find a close correspondence between D_{max} and L_{EK}, except a short period centered around May 14 (shaded area in Figure 2a; with generally high r^2 values ($r^2 = 0.66$ over the non-shaded portion of the record) and low root mean square differences, (rmsd) between D_{max} and L_{EK} (22.2 m, compared with an average D_{max} of 48.7 m and a range in D_{max} over the float record of 150.0 m.)

In the buoyancy-driven case (the 1997 Labrador Sea record over 20 February to 7 March, Figure 2b), D_{max} is of comparable magnitude with H, but only when H is defined using the 0.03 kg m^{-3} density difference criterion. Again, the rmsd between H and D_{max} is small (279 m) compared with the average depth of D_{max} (635 m) and range over the period and floats (754 m). The correlation between D_{max} and H on any given day is low ($r^2 = 0.024$), but because H is calculated using density profiles from PALACE floats, which are close to, but not at, the position of the Lagrangian floats, D_{max} is averaged from several Lagrangian float records, and the Labrador Sea record is relatively short and does not record large changes in D_{max} or H, this low correlation can be

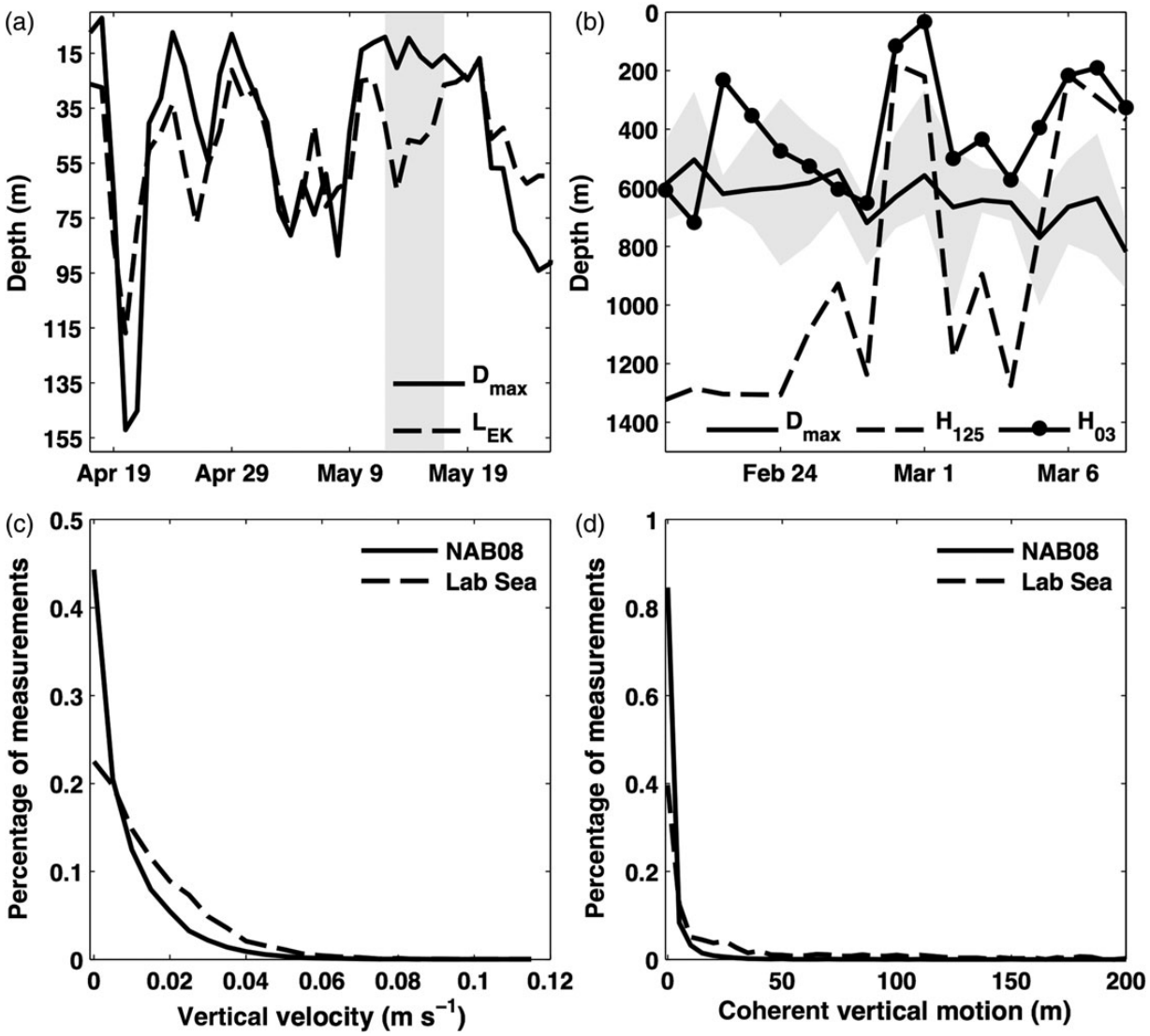

Figure 2. (a) Daily maximum depths attained by the NAB08 float (D_{max}), compared with the Ekman depth (L_{EK}). Grey shading is as in Figure 3c. (b) Daily maximum depths averaged over the four Lab Sea floats with complete records (Floats 8, 12, 16, and 21) (D_{max}), compared with the mixed layer depths H_{03} and H_{125}. The grey shading denotes the daily minimum/maximum of D_{max} out of the four floats. (c) Normalized distributions of the magnitude of float vertical velocities for the Labrador Sea and NAB08 data. Distributions were created using bin sizes of 0.005, ranging from 0 to 0.115 m s^{-1}, with open boundaries. (d) Normalized distributions of the magnitude of coherent vertical motions recorded by the floats. Distributions were created using bin sizes of 5, ranging from 0 to 300 m, with open boundaries. For all distributions in (c, d), the Labrador Sea distribution is composed of the four Labrador Sea floats shown in (b).

expected. Nonetheless, in both the wind-driven and buoyancy-driven case, we find support for the BL14 estimation of the active mixing depth.

Comparison of buoyancy- and wind-driven mixing

We next explore whether the large difference between the depth of the active mixing layer in the buoyancy-driven and the wind-driven mixing regimes (Figure 2a and b) is accompanied by differences in the magnitude of the vertical velocities, and the size of coherent vertical motions. The distributions of the magnitude of turbulent vertical velocity measurements, $|w'|$ (Figure 2c), in the two experiments show that floats in the buoyancy-driven mixing environment have a higher mean $|w'|$ (0.016 m s^{-1} compared with 0.010 m s^{-1}) and a larger variance (1.97×10^{-4} m s^{-1} compared with 1.26×10^{-4} m s^{-1}).

The distributions of the coherent vertical motions, i.e. the magnitude of the vertical distance travelled by a float before changing directions, for both the buoyancy-driven and wind-driven mixing environments (Figure 2d), show that in the buoyancy-driven case, the floats more frequently record large vertical motions. In this case, the variance of the buoyancy-driven distribution is several orders of magnitude greater than the wind-driven distribution (8.82×10^{-3} vs. 4.28×10^{-5} m). The mean of the buoyancy-driven vertical motions is also much greater (47.8 vs. 2.81 m). For both the distributions of $|w|$ and the coherent vertical motions, Kolmogorov–Smirnov tests (Massey, 1951) show that the distributions of the NAB08 and Lab Sea data are significantly different at the

95% confidence level. These comparisons support the idea that the deep active mixing layers observed in the buoyancy-driven mixing environment result from large coherent convective cells, in contrast to the smaller motions that characterize the wind-driven regime.

Analysis of L_{mix} and bloom initiation

The NAB08 record provides the opportunity to examine changes in turbulent vertical velocities and the depth of L_{mix} before and during the initiation of a subpolar spring bloom. The bloom initiation date occurs on Day 12 of the NAB08 record (16 April, Figure 3a), approximately 2 d before heat fluxes become positive (Figure 3a). This timing is consistent with the analysis of Mahadevan *et al.* (2012), who approximated the NAB08 bloom initiation date from the biomass record, and with BL14, who found positive satellite-derived chlorophyll rates of change in the subpolar North Atlantic to occur when heat fluxes were weakening but still negative.

As noted in Mahadevan *et al.* (2012), and as seen at other study sites (D'Asaro, 2003), daily rms-vertical velocities calculated from the Lagrangian float data (w_{rms}) and turbulent vertical velocities calculated from wind stress (w^*) are generally in very good agreement (Figure 3b), indicating the dominance of wind-driven mixing during the bloom initiation. However, this correspondence is weak during approximately the first 9 d of the time series, before the bloom initiation, when w_{rms} is significantly larger than and less correlated with w^* as compared with the remainder of the

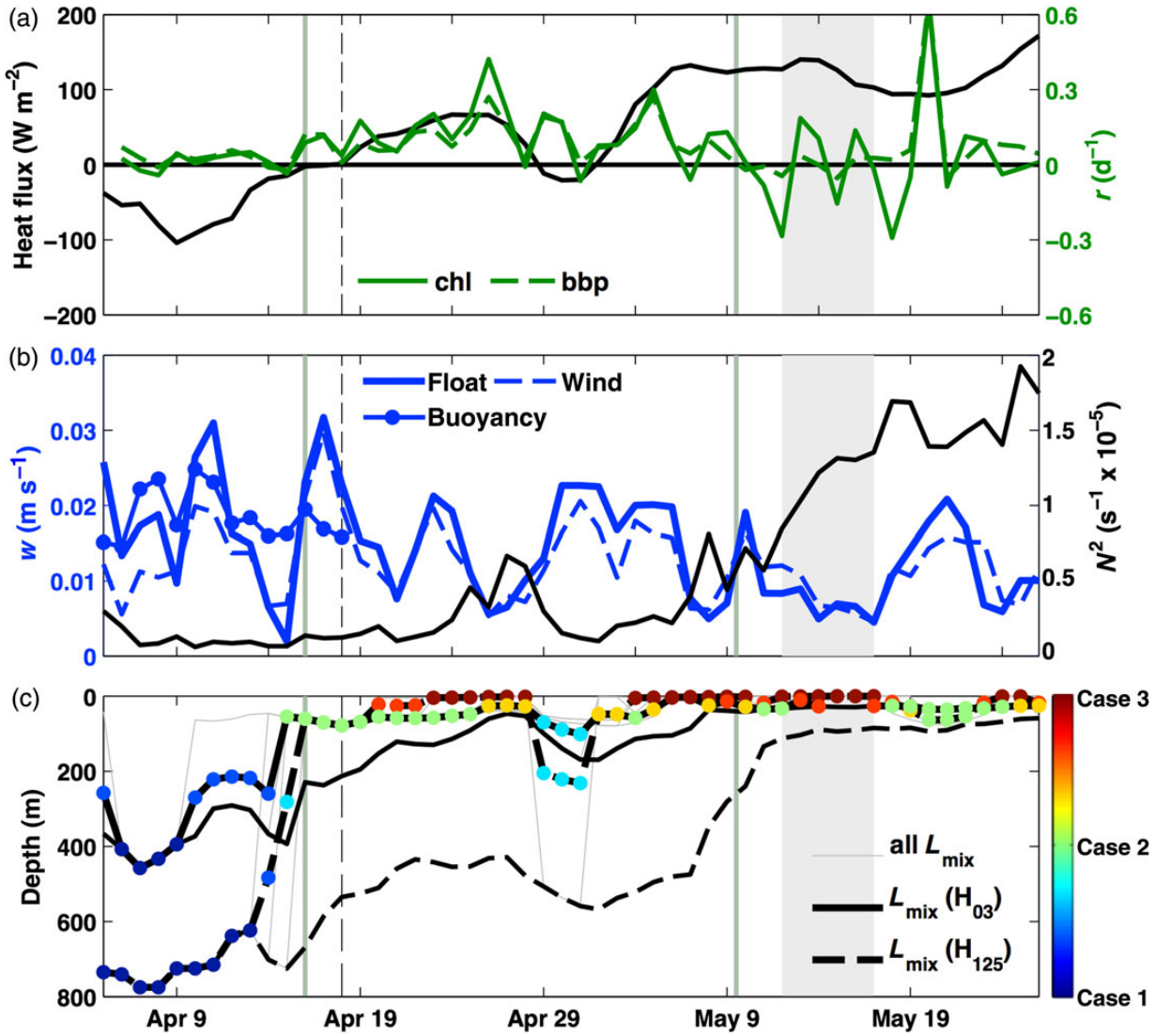

Figure 3. (a) Daily rates of change (r) of depth-integrated chlorophyll fluorescence and bbp(700) measured from NAB08 glider profile data, plotted with heat fluxes averaged from the OAFLUX, NCEP-NCAR, and ECMWF-ERA products. The vertical green lines show the dates on which r becomes consistently positive (the bloom initiation) and negative (the bloom termination). The vertical black line shows the date on which the averaged heat flux time series becomes positive. (b) Turbulent vertical velocities calculated from the WaveWatch III windstress record, the daily averaged buoyancy flux record, and derived from rms daily averaged vertical float velocities. (c) L_{mix} depth measurements shown calculated for all possible combinations of the OAFLUX, NCEP-NCAR, and ECMWF-ERA heat flux/wind products and mixed layer depth definitions, then averaged for H_{03} and H_{125}. Marker colours refer to the case (1, 2, or 3) of L_{mix} at each day, averaged for the L_{mix} measurements calculated from all three surface forcing products. The H_{03} and H_{125} are also shown as the non-markered solid and dashed lines.

NAB08 record (Table 1). This period coincides with a period of relatively strong loss of heat to the atmosphere (Figure 3a); thus, buoyancy forcing is potentially playing a role in the turbulent mixing during this time. We estimate buoyancy-driven vertical velocities (w_b) for the entire period of negative heat fluxes (the first 14 d of the float record, Figure 3b). Because of the lower spatial resolution of the heat flux data when compared with the wind data, and because of the additional uncertainty introduced by the glider-derived mixed layer depths in the calculation of w_b, we expect generally lower correlations between w_b and w_{rms} than between w^* and w_{rms}. However, we do see that during the first 9 d of the record, the correlation between w_b and w_{rms} is higher than during the bloom initiation (Days 10–14), when heat fluxes are weak, while the correlation between w^* and w_{rms} is higher during Days 10–14 than Days 1–9 (Table 1). The rmsd between w_b and w_{rms} is also lower during the first 9 d of the record compared with the rmsd between w^* and w_{rms} during this period (Table 1). These patterns support the hypothesis that mixing is not wind-driven, and may be buoyancy-driven, before the bloom initiation.

A shift from buoyancy-driven to wind-driven mixing occurring 3 d before the start of the bloom would be consistent with the bloom initiation framework developed in BL14. Moreover, the average stratification over the portion of the water column in which the Lagrangian float travels stays very low until well after the bloom initiation (Figure 3b), also consistent with the BL14 idea that the bloom begins during Case 2 mixing (wind-driven mixing in unstratified conditions). We note, however, that the relatively short period during which heat fluxes were strongly negative and stratification was low, as well as the small number of days in which heat fluxes were weakly negative, precludes a definitive assessment of the drivers of mixing before the bloom.

The hypothesis that a shift from buoyancy-driven to wind-driven mixing creates the conditions in which a bloom can begin rests on the assumption that this shift decreases the depth of active mixing. The model for this active mixing depth, L_{mix}, contains different parameterizations for buoyancy-driven mixing (Case 1, $L_{mix} = H$) and wind-driven mixing (Case 2, $L_{mix} = L_{EK}$). We next examine whether L_{mix} calculated over the period of the NAB08 record transitions from Case 1 to Case 2 synchronously with the observed shift in the w_{rms} record from w_b-correlated with w^*-correlated, and, if so, whether this transition causes L_{mix} to shoal. All L_{mix} estimates show a clear shift from Case 1 to Case 2 coincident with bloom initiation (Figure 3c) and with the beginning of increased correspondence between w^* and w_{rms} (Figure 3b). This shift from Case 1 to Case 2 is accompanied by a large decrease in L_{mix}, consistent with the idea that such a decrease leads to an increase in light availability for phytoplankton and thus drives the spring bloom. During the same period, mixed layers generally remain very deep, and do not show the same pronounced shoaling seen in the L_{mix} record (Figure 3c).

During most of the remainder of the bloom period, the close correspondence between w^* and w_{rms} (Figure 3b), the relatively weak heat fluxes (Figure 3a), the strong agreement between the float-derived D_{max} and estimated L_{EK} (Figure 3a), and the weak stratification (Figure 3b) indicate that Case 2 conditions prevail. During the period of approximately 12 May through 18 May (after the bloom termination, shaded area in Figure 3c), the overestimation of D_{max} by L_{EK} (Figure 2a), the slight overestimation of w_{rms} by w^* (Figure 3b), and the relatively high stratification (Figure 3b) indicate that L_{mix} is in Case 3, or stratified wind-driven mixing. While L_{mix} calculated using H_{03} generally follows this pattern, L_{mix} calculated using H_{125} transitions to Case 3 well before 12 May, indicating that H_{03} is the more appropriate definition of the mixed layer depth for the calculation of L_{mix} in the NAB08 location and period.

The depth-resolved NAB08 glider data provide additional evidence that the phytoplankton bloom initiation corresponds to the shoaling of L_{mix}, rather than to the shoaling of the mixed layer. We compare L_{mix} calculated using H_{03} with both H_{03} and with the depths of the euphotic depth and threshold isolume (z_{eu}, z_{415}), again using depth-time profiles of both chlorophyll fluorescence and bbp(700) as proxies for phytoplankton biomass (Figure 4). Before the initiation of the spring bloom, H and L_{mix} are equal and very deep. Phytoplankton biomass, as measured by both chlorophyll fluorescence (Figure 4a) and bbp(700) (Figure 4b), is distributed fairly evenly over the top 300–400 m of the water column. At this point, H_{03} and L_{mix} both approximate the bottom boundary of biomass accumulation, as expected for pre-bloom, buoyancy-mixed conditions. At and directly after the bloom initiation date, the chlorophyll fluorescence and bbp(700) depth profiles noticeably increase in concentration within the top 50–100 m. L_{mix}, which has shoaled considerably, generally tracks these horizons. Though H_{03} shoals during this period, it remains deeper than the highest concentrations of biomass.

As the bloom progresses and reaches its termination date, chlorophyll fluorescence and bbp(700) concentrations are approximately uniform and high within the top 50–150 m of the record (Figure 4). While L_{mix} and H_{03} intermittently shoal above these concentration horizons, the euphotic depth and threshold isolume begin to delineate the bottom boundary of significant biomass growth and accumulation. The records during this period also show evidence of sinking biomass, particularly in the elevated bbp(700) concentrations after 1 May (dashed line in Figure 4b) and in the chlorophyll fluorescence and bbp(700) spike at 300–400 m on 9 May, which was analysed by Briggs *et al.* (2011) for its role in carbon export. Because sinking biomass creates a vertical profile that indicates increased concentration at depth, yet that concentration includes the non-growing population, we place greater emphasis on the match between L_{mix} and biomass at the beginning of the bloom.

Table 1. Correlation (r^2) and difference (rmsd) information for wind-estimated and buoyancy-estimated vertical velocities compared with the observed vertical velocities (w_{rms}) for different segments of the NAB08 record.

	Days 1–9	Days 10–14	Days 10–52
w^*	0.51, 0.0078	0.97, 0.0029	0.82, 0.0032
w_b	0.24, 0.0058	0.14, 0.0107	NA

[a]The first number in each box denotes the r^2 value for each velocity and time segment; the second number denotes the rmsd value (units ms^{-1}).
[b]There is no value for buoyancy-estimated vertical velocities during Days 10–52 because buoyancy-estimated velocities are only computed when heat fluxes are negative.

Discussion

In this study, we used *in situ* data to further examine the light-limitation-based mechanisms for subpolar bloom initiation first formalized by the Sverdrup Hypothesis. Specifically, we examined the idea that phytoplankton are uniformly mixed to the depth of the dominant mixing length scale, or active mixing depth (L_{mix}), which shoals during the transition from buoyancy- to wind-driven

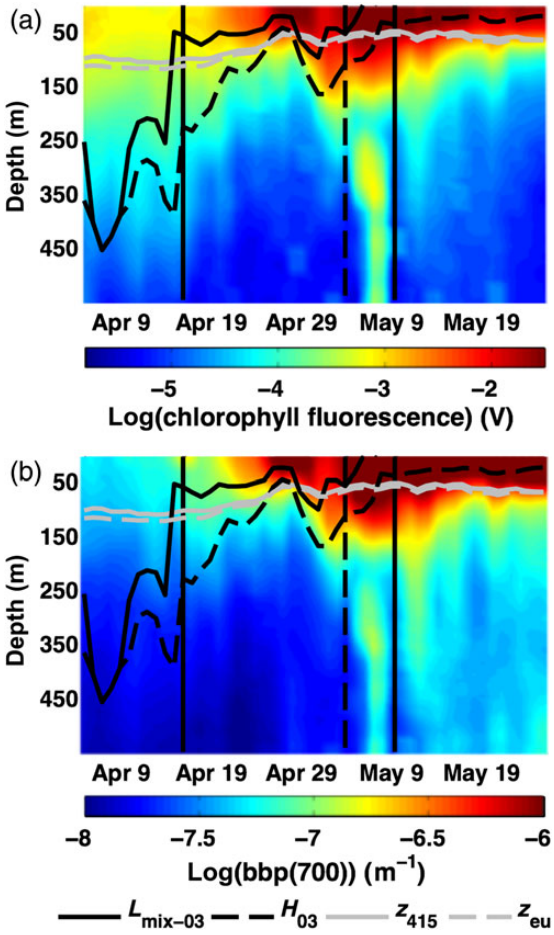

Figure 4. Daily chlorophyll fluorescence (a) and bbp(700) concentration (b) depth-time records from the NAB08 glider data. Both records are plotted on a log scale. In both plots, the time span shown is the same as in Figure 3, the black vertical solid lines correspond to the bloom initiation and termination dates shown as green lines in Figure 3, and the black vertical dashed lines highlight the beginning of apparent biomass sinking (1 May). The threshold isolume (z_{415}) used to calculate r and euphotic depth (z_{eu}) are also shown.

mixing, thus alleviating light limitation and prompting a bloom. This idea is consistent with previous observations made of blooms occurring when heat fluxes are negative (Mahadevan *et al.*, 2012) and when the water column is unstratified (Townsend *et al.*, 1992).

We first examined whether the BL14 estimation of L_{mix} from surface forcing data accurately estimates the depth of active mixing in buoyancy- and wind-driven mixing regimes. According to the BL14 framework, L_{mix} should be equal to the mixed-layer depth, H, during buoyancy-driven mixing and equal to the Ekman depth, L_{EK}, during wind-driven mixing. We found that the daily maximum depths attained by the Lagrangian floats in these regimes are consistent with H_{03} for buoyancy-driven regimes and with L_{EK} for wind-driven regimes (Figure 2a and b).

A further investigation of the wind-driven record in the context of the spring bloom shows that the daily maximum float depth corresponds very closely to L_{EK}, or Case 2 mixing, during the initiation and duration of the bloom (17 April–9 May). The daily maximum depths then become more shallow than L_{EK} for a brief period after the bloom termination (12 May–18 May), indicating a shift to Case 3 mixing. This shift is also seen in the relatively high heat fluxes (Figure 3a), low observed turbulent vertical velocities (Figure 3b), and high stratification (Figure 3b) at this time. That this shift is mirrored in the L_{mix} record, which briefly transitions to Case 3 from Case 2 on these days (Figure 3c), provides further support for L_{mix} as an estimator of the depth of active mixing.

We explored in more detail the differences and similarities between buoyancy-driven and wind-driven mixing, as seen in the Lagrangian float records. The deep maximum depths, high vertical velocities, and large coherent vertical motions experienced by floats in the buoyancy-driven environment, compared with those in the wind-driven environment (Figure 2), support the hypothesis that coherent convective cells within the mixed-layer drive deeper mixing of particles when mixing is generated by buoyancy forcing.

Further, we found evidence to support the idea that mixing transitions from buoyancy-driven to wind-driven in the NAB08 record shortly before the bloom begins. Wind-estimated turbulent vertical velocities (w^*) underestimate observed vertical velocities (w_{rms}) before the bloom initiation. During the same period, heat fluxes are negative and the correspondence between w_{rms} and buoyancy-estimated velocities (w_b) is relatively high (Table 1, Figure 3b).

Finally, we find significant shoaling of L_{mix} to coincide with both the increased synchrony between the wind-estimated and observed vertical velocities and the beginning of the spring bloom, in contrast to the density-defined mixed layer during this period (Figure 3c). We find further evidence of this synchrony in depth-resolved biomass time series (Figure 4), in which L_{mix} better delineates the lower boundary of increased surface biomass concentrations at the onset of the bloom than does the density-defined mixed layer.

Our results thus support the underlying ideas of the Sverdrup hypothesis—that phytoplankton are uniformly mixed to deep depths in winter, with little available light, then begin to bloom in spring as mixing weakens and the population concentrates in the light-filled upper ocean. At the same time, we propose that decreases in the dominant mixing length scales operating in the upper ocean (L_{mix}), driven by the transition from buoyancy-driven to wind-driven mixing, better predict the onset of the spring bloom than the surface warming and consequent decreases in the density-defined mixed layer typically attributed to the Sverdrup hypothesis. Given that the Sverdrup hypothesis is predicated on the phytoplankton mixing depth shoaling above the critical depth (where integrated phytoplankton photosynthesis equals integrated respiration) before the bloom, the critical depth during the NAB08 experiment might be located between 250 and 50 m, the approximate depths of L_{mix} before and after it shoals.

We further note that at and after the bloom termination, depth-resolved profiles show high concentrations of biomass deeper than either the density-defined mixed layer or L_{mix} would predict (Figure 4). It has been suggested that in stratified, high-light conditions, phytoplankton grow to the depth of the euphotic zone, deeper at these times than the depth of surface mixing (Behrenfeld, 2010; Boss and Behrenfeld, 2010). Our results confirm this idea, providing justification for integrating biomass to the depth of a threshold isolume to calculate rates of change during these periods (Behrenfeld, 2010), as we do here to calculate r, and suggesting that the highest phytoplankton growth does not occur within the active mixing layer year-around. Additionally, our analysis makes it apparent that, for both the Labrador Sea and NAB08 data, the

mixed layer based on the 0.03 kg m^{-3} density threshold, and by extension the Holte-Talley algorithm mixed layer depth, is noticeably more appropriate for the active mixing depth estimation than the 0.125 kg m^{-3} threshold. While this may not be the case for all datasets and regions, the mixed-layer depth definition used to calculate L_{mix} must always be chosen deliberately.

While our work provides evidence for the idea that the shift from buoyancy-driven to wind-driven mixing, reflected in the shoaling of L_{mix}, provides the necessary mechanism for bloom initiation at the NAB08 site, recent studies have offered different explanations for the subpolar spring bloom. Mahadevan *et al.* (2012) also used the NAB08 data and, noting the appearance of a bloom before heat fluxes became positive, used the record of shallow vs. deep stratification, as well as a numerical model, to propose that mixed-layer eddies, arising from horizontal density gradients, drive stratification, and bloom initiation before the warming of the ocean surface. We use the same *in situ* data, though with stratification measured over a different part of the water column, to propose that changes in surface forcing and one-dimensional mixing alone are sufficient to drive bloom initiation. However, perhaps both of these proposed mechanisms could be at play at different times and to different extents throughout the subpolar oceans in the early spring. We note that the stratification signature observed by Mahadevan *et al.* (2012) in the NAB08 record—a concurrent, small increase in shallow and deep stratification while heat fluxes are negative followed by a large increase in shallow stratification only after heat fluxes become positive, is consistent with a stratification scenario that might be observed in the transition from Case 2 to Case 3 mixing in our formulation.

A theory of bloom initiation based on top-down control of phytoplankton has also been proposed (Behrenfeld, 2010; Boss and Behrenfeld, 2010; Behrenfeld *et al.*, 2013): that deep mixed-layers dilute plankton populations, reduce encounters between zooplankton grazers and phytoplankton, and thus promote growth in the integrated population. This theory has been tested *in situ* as well, using data from an optical profiling float released in the North Atlantic between 2004 and 2007 between 45 and 55°N (Boss *et al.*, 2008; Boss and Behrenfeld, 2010). However, two factors prevent a direct comparison with the NAB08 data. First, this float profiled an area of the North Atlantic 5–10° southward of the NAB08 experiment site, where the average PAR over the course of a year is significantly higher than at the NAB08 site, and productivity patterns are indicative of the transition zone between subtropical and subpolar waters, where light limitation is not the sole driver of phytoplankton blooms (Brody *et al.*, 2013). Relatedly, the mixed layers recorded by that float, determined using the 0.125 kg m^{-3} density difference criterion, never exceeded 160 m, and usually stayed >100 m, vastly increasing the winter light exposure of the biomass in that area compared with the biomass experiencing the 700–800 m mixed layers observed at the beginning of the NAB08 record. While it is possible that, had the NAB08 experiment started during winter, rather than at the beginning of April, it would have recorded growth in the integrated population as mixed layers deepened, it is equally possible that light limitation becomes a more important factor than dilution and grazing in setting the timing of the phytoplankton bloom in areas of deep mixed layers and low winter PAR.

Thus, from available data, there is strong *in situ* evidence for decreases in L_{mix}, driven by a shift from buoyancy-driven to wind-driven mixing, as one of the primary drivers of the subpolar spring phytoplankton bloom. This formulation of the light-limitation-based theory for subpolar blooms raises the possibility that changes in ocean-atmosphere forcing conditions on interannual to decadal timescales, as they affect the timing of the transition from buoyancy to wind-driven mixing, could affect the timing of the spring phytoplankton bloom in a predictable manner.

References

Behrenfeld, M. 2010. Abandoning Sverdrup's critical depth hypothesis on phytoplankton blooms. Ecology, 91: 977–989.

Behrenfeld, M., Boss, E., Siegel, D., and Shea, D. 2005. Carbon-based ocean productivity and phytoplankton physiology from space. Global Biogeochemical Cycles, 19: GB1006.

Behrenfeld, M., Doney, S., Lima, I., Boss, E., and Siegel, D. 2013. Annual cycles of ecological disturbance and recovery underlying the subarctic Atlantic spring plankton blooms. Global Biogeochemical Cycles, 27: 526–540.

Boss, E., and Behrenfeld, M. 2010. In situ evaluation of the initiation of the North Atlantic phytoplankton bloom. Geophysical Research Letters, 37: L18603.

Boss, E., Swift, L., Taylor, L., Brickley, P., Zaneveld, R., Riser, S., Perry, M., *et al.* 2008. Observations of pigment and particle distributions in the western north Atlantic from an autonomous float and ocean color satellite. Limnology and Oceanography, 53: 2112–2122.

Briggs, N., Perry, M., Cetinic, I., Lee, C., D'Asaro, E., Gray, A., and Rehm, E. 2011. High-resolution observations of aggregate flux during a subpolar North Atlantic spring bloom. Deep-Sea Research Part I, 58: 1031–1039.

Brody, S., and Lozier, M. 2014. Changes in dominant mixing length scale as a driver of phytoplankton bloom initiation in the North Atlantic. Geophysical Research Letters, 41: 3197–3206.

Brody, S., Lozier, M., and Dunne, J. 2013. A comparison of methods to determine phytoplankton bloom initiation. Journal of Geophysical Research: Oceans, 118: 2345–2357.

Cetinic, I., Perry, M., Briggs, N., Kallin, E., D'Asaro, E., and Lee, C. 2012. Particulate organic carbon and inherent optical properties during 2008 North Atlantic bloom experiment. Journal of Geophysical Research, 117: C06028.

Chiswell, S. 2011. Annual cycles and spring blooms in phytoplankton: don't abandon Sverdrup completely. Marine Ecology Progress Series, 443: 39–50.

Chiswell, S., Bradford-Grieve, J., Hadfield, M., and Kennan, S. 2013. Climatology of surface chlorophyll *a*, autumn-winter and spring blooms in the southwest Pacific Ocean. Journal of Geophysical Research, 118: 1–16.

Cole, H., Henson, S., Martin, A., and Yool, A. 2012. Mind the gap: the impact of missing data on the calculation of phytoplankton phenology metrics. Journal of Geophysical Research, 117: C08030.

D'Asaro, E. 2003. Performance of autonomous Lagrangian floats. Journal of Atmospheric and Oceanic Technology, 20: 896–911.

D'Asaro, E. 2008. Convection and seeding of the North Atlantic bloom. Journal of Marine Systems, 69: 233–237.

D'Asaro, E., Farmer, D., Osse, J., and Dairiki, G. 1996. A Lagrangian float. Journal of Atmospheric and Oceanic Technology, 13: 1230–1246.

Davis, R., Regier, L., Dufour, J., and Webb, D. 1992. The autonomous Lagrangian circulation explorer (ALACE). Journal of Atmospheric and Oceanic Technology, 9: 264–285.

Deardorff, J. 1972. Numerical investigations of neutral and unstable planetary boundary layers. Journal of Atmospheric Science, 29: 91–115.

Deardorff, J., and Willis, G. 1985. Further results from a laboratory model of the convective planetary boundary layer. Boundary Layer Meteorology, 32: 205–236.

Denman, K., and Gargett, A. 1983. Time and space scales of vertical mixing and advection of phytoplankton in the upper ocean. Limnology and Oceanography, 28: 801–815.

Edwards, M., and Richardson, J. 2004. Impact of climate change on marine pelagic phenology and trophic mismatch. Nature, 430: 881–884.

Eriksen, C., Osse, T., Light, R., Wen, T., Lehman, T., Sabin, P., Ballard, J., *et al.* 2001. Seaglider: a long-range autonomous underwater vehicle for oceanographic research. IEEE Journal of Oceanic Engineering, 26: 424–436.

Fennel, L., Cetinic, I., D'Asaro, E., Lee, C., and Perry, M. 2011. Autonomous data describe North ATLANTIC spring bloom. Eos Transactions, 92: 465–466.

Fernando, H., Chen, R., and Boyer, D. 1991. Effects of rotation on convective turbulence. Journal of Fluid Mechanics, 228: 513–547.

Follows, M., and Dutkiewicz, S. 2001. Meteorological modulation of the North Atlantic spring bloom. Deep-Sea Research Part II, 49: 321–344.

Harcourt, R., Steffen, E., Garwood, R., and D'Asaro, E. 2002. Fully Lagrangian floats in Labrador Sea deep convection: comparison of numerical and experimental results. Journal of Physical Oceanography, 32: 493–510.

Henson, S., Dunne, J., and Sarmiento, J. 2009. Decadal variability in North Atlantic phytoplankton blooms. Journal of Geophysical Research, 114: C04013.

Henson, S., Robinson, I., Allen, J., and Waniek, J. 2006. Effect of meteorological conditions on interannual variability in timing and magnitude of the spring bloom in the Irminger Basin, North Atlantic. Deep Sea Research Part I, 53: 1601–1615.

Hersbach, H. 2011. Sea surface roughness and drag coefficient as a function of neutral wind speed. Journal of Physical Oceanography, 41: 247–251.

Holte, J., and Talley, L. 2009. A new algorithm for finding mixed layer depths with applications to Aego data and subantarctic mode water formation. Journal of Atmospheric and Oceanic Technology, 26: 1920–1939.

Huisman, J., van Oostveen, P., and Weissing, F. 1999. Critical depth and critical turbulence: two different mechanisms for the development of phytoplankton blooms. Limnology and Oceanography, 44: 1781–1787.

Kanamitsu, M., Ebisuzaki, W., Woollen, J., Yang, S.-K., Hnilo, J., Fiorino, M., and Potter, G. 2002. NCEP-DEO AMIP-II reanalysis (R-2). Bulletin of the American Meteorological Society, 83: 1631–1643.

Koeller, P., Fuentes-Yaco, C., Platt, T., Sathyendranath, S., Richards, A., Ouellet, P., Orr, D., *et al.* 2009. Basin-scale coherence in phenology of shrimps and phytoplankton in the North Atlantic Ocean. Science, 324: 791–793.

Krahmann, G., Visbeck, M., Smethie, W., D'Asaro, E., Rhines, P., Clarke, R., Lazier, J., *et al.* 2003. The Labrador Sea deep convection experiment data collection. Geochemistry Geophysics Geosystems, 4: 4.

Lavender, K., Davis, R., and Owens, W. 2000. Mid-depth recirculation observed in the interior Labrador and Iringer seas by direct velocity measurements. Nature, 407: 66–69.

Letelier, R., Karl, D., Abbot, M., and Bidigare, R. 2004. Light driven seasonal patterns of chlorophyll and nitrate in the lower euphoric zone of the North Pacific subtropical gyre. Limnology and Oceanography, 49: 508–519.

Lutz, M., Caldeira, K., Dunbar, R., and Behrenfeld, M. 2007. Seasonal rhythms of net primary production and particulate organic flux to depth describe the efficiency of the biological pump in the global ocean. Journal of Geophysical Research, 112: C10011.

Mahadevan, A., D'Asaro, E., Lee, C., and Perry, M. 2012. Eddy-driven stratification initiates North Atlantic spring phytoplankton blooms. Science, 337: 54–58.

Massey, F. 1951. The Kolmogorov-Smirnov test for goodness of fit. Journal of the American Statistical Association, 46: 68–78.

McDougall, T., and Barker, P. 2011. Getting started with TEOS-10 and the Gibbs Seawater (GSW) Oceanographic Toolbox.

Molemaker, M., and Dijkstra, H. 1997. The formation and evolution of a diffusive interface. Journal of Fluid Mechanics, 331: 199–229.

Morel, A., Huot, Y., Gentili, B., Werdell, P., Hooker, S., and Brayan, A. 2007. Examining the consistency of products derived from various ocean color sensors in open ocean (case 1) waters in the perspective of a multi-sensor approach. Remote Sensing of Environment, 111: 69–88.

Phillips, O. 1977. The Dynamics of the Upper Ocean. Cambridge University Press, Cambridge, UK, and New York.

Platt, T., Fuentes-Yaco, C., and Frank, K. 2003. Spring algal bloom and larval fish survival. Nature, 423: 398–399.

Platt, T., White, G., 3rd, Zhai, L., Sathyendranath, S., and Roy, S. 2009. The phenology of phytoplankton blooms: ecosystem indicators from remote sensing. Ecological Modeling, 220: 3057–3069.

Racault, M., Le Quéré, C., Buitenhuis, E., Sathyendranath, S., and Platt, T. 2012. Phytoplankton phenology in the global ocean. Ecological Indicators, 14: 152–163.

Riley, J., and Lelong, M. 2000. Fluid motions in the presence of strong stable stratification. Annual Reviews of Fluid Mechanics, 32: 613–657.

Sabine, C., Feely, R., Gruber, N., Key, R., Lee, K., Bullister, J., Wanninkhof, R., *et al.* 2004. The oceanic sink for anthropogenic CO2. Science, 305: 367–371.

Sapiano, M., Brown, C., Schollaert Uz, S., and Vargas, M. 2012. Establishing a global climatology of marine phytoplankton phenological characteristics. Journal of Geophysical Research, 117: C028026.

Siegel, D., Doney, S., and Yoder, J. 2002. The North Atlantic spring phytoplankton bloom and Sverdrup's critical depth hypothesis. Science, 296: 730–733.

Steffen, E., and D'Asaro, E. 2002. Deep convection in the Labrador Sea as observed by Lagrangian floats. Journal of Physical Oceanography, 32: 475–492.

Stramska, M., Dickey, T., Plueddemann, A., Weller, R., Langdon, C., and Marra, J. 1995. Bio-optical variability associated with phytoplankton dynamics in the North Atlantic Ocean during spring and summer of 1991. Journal of Geophysical Research, 100: 6621–6632.

Sverdrup, H. 1953. On conditions for the vernal blooming of phytoplankton. Journal du Conseil International Pour L'Exploration de la Mer, 18: 287–295.

Taylor, J., and Ferrari, R. 2011. Shutdown of turbulent convection as a new criterion for the onset of spring phytoplankton blooms. Limnology and Oceanography, 56: 2293–2307.

Townsend, D., Keller, M., Sieracki, M., and Ackleson, S. 1992. Spring phytoplankton blooms in the absence of vertical water column stratification. Nature, 360: 59–62.

Wang, W., and Huang, R. 2003. Wind energy input the Ekman layer. Journal of Physical Oceanography, 34: 1267–1275.

Yu, L., and Weller, R. 2007. Objectively analyzed air-sea heat fluxes for the global ice-free oceans (1981–2005). Bulletin of the American Meteorological Society, 88: 527–539.

Handling editor: Shubha Sathyendranath